Mapping Burned Areas in a Mediterranean Environment Using Soft Integration of Spectral Indices from High-Resolution Satellite Images

Mirco Boschetti,* Daniela Stroppiana, and Pietro Alessandro Brivio

Institute for Electromagnetic Sensing of the Environment (IREA), National Research Council (CNR), Milan, Italy

ABSTRACT: This article presents a new method for burned area mapping using high-resolution satellite images in the Mediterranean ecosystem. In such a complex environment, high-resolution satellite images represent an appropriate data source for identifying fire-affected areas, and single postfire data are often the only available source of information. The method proposed here integrates several spectral indices into a fuzzy synthetic indicator of likelihood of burn. The indices are interpreted through fuzzy membership functions that have been derived with a partially data-driven approach exploiting training data and expert knowledge. The final map of fire-affected areas is produced by applying a region growing algorithm on the basis of seed pixels selected on a conservative threshold of the synthetic fuzzy score. The algorithm has been developed and tested on a set of Advanced Spaceborne Thermal Emission and Reflection Radiometer (ASTER) scenes acquired over Southern Italy. Validation showed that the accuracy of the burned area maps is comparable or even better [overall

---

* Corresponding author address: Mirco Boschetti, IREA-CNR, Institute for Electromagnetic Sensing of the Environment, National Research Council, Via Bassini 15, 20133 Milan, Italy.

E-mail address: boschetti.m@irea.cnr.it

accuracy (OA) > 90%, *K* > 0.76] than that obtained with approaches based on single index thresholds adapted to each image. The method described here provides an automatic approach for mapping fire-affected areas with very few false alarms (low commission error), whereas omission errors are mainly related to undetected small burned areas and are located in heterogeneous sparse vegetation cover.

1. Introduction

Fire is a significant source of gas and aerosols worldwide (French et al. 2003) and an important disturbance factor for the ecosystems that induces land-cover modification and change (Thonicke et al. 2001). Since the late 1990s, Earth observation (EO) data have been extensively used for active fire mapping (i.e., presence of the flaming front or ''hot spot''; Dwyer et al. 1998; Arino and Rosaz 1999; Giglio et al. 2003) and for delimiting burned area perimeters (Barbosa et al. 1998; Simon et al. 2004; Tansey et al. 2004; Roy et al. 2005). More recently, satellite data have been used to characterize fire events through the retrieval of the power released by fire [i.e., fire radiative power (FRP); Wooster et al. 2003].

Medium-/coarse-resolution (MR; 500–1000 m) satellite data, such as the *Terra/Aqua* Moderate Resolution Imaging Spectrometer (MODIS), National Oceanic and Atmospheric Administration (NOAA)/Advanced Very High Resolution Radiometer (AVHRR), and Satellite Pour l'Observation de la Terre (SPOT) VEGETATION (VGT), have been exploited to build a long time series of fire-related information over large areas, on both continental and global scales (Pu et al. 2007; Stroppiana et al. 2003), and are generally used for atmosphere studies such as those related to the carbon cycle and climate change (Van der Werf et al. 2006).

High-resolution (HR; 15–30 m) images, such as those provided by the Landsat Thematic Mapper (TM), SPOT High Resolution Geometric (HRG) instrument, or Indian Remote Sensing (IRS) satellite Linear Imaging Self Scanning Sensor (LISS-3), are generally used for building reference datasets for accuracy assessment of the medium/coarse burned area maps (Silva et al. 2005) and for providing fire perimeters on a regional/local scale (Kontoes et al. 2009).

Very high-resolution (VHR; 1–5 m) images, such as *IKONOS* or *QuickBird*, have been successfully used with object-oriented techniques to detect burned areas and fire typology (Mitri and Gitas 2006). These data provide very detailed thematic products and are very helpful for studying a single or a few fire events. However, because of the small dimension of the satellite swath (about 10 km) and the acquisition policies, which do not guarantee systematic acquisitions, VHR data are not suitable for regional monitoring.

In the Mediterranean environment, which is characterized by a complex and fragmented structure of the landscape and the heterogeneity of the land cover, burned areas are generally small. Analysis of the official reports [European Forest Fire Information System (EFFIS)] compiled for five Mediterranean countries (Portugal, Spain, France, Italy, and Greece) during a 30-yr period indicates an average fire size of 10 ha with a minimum of 6 ha for Portugal and France, a maximum of 30 ha for Greece, and a value of 11 ha for Spain and Italy (Camia et al. 2009). In Italy, fires get particularly intense in the southern regions of the

country. In the last decade, the worst year was 2007, when the vegetated surface hit by fires amounted to 227.729 ha, even larger than Greece (225.734 ha), although fires caused less human causalities. Examination of the EFFIS database highlighted also that fire in Europe is mainly a human-induced phenomenon: up to 95% of fires are directly (51% intentionally) or indirectly (44% accident/negligence) caused by human behavior and activities (Catry et al. 2010).

Most of the Mediterranean countries, which are affected by forest fires, do not have proper data on fire incidence (Paganini et al. 2003). Also in Italy, consistent historical archives on burned area perimeters are not available, because fire monitoring has been traditionally carried out on the basis of qualitative field observations conducted by forest guards and fire brigades. The analysis of satellite images is the only method to fill the gaps of historical datasets, which rely only on field observations. Some initiatives have been carried out on a national scale for exploiting satellite data for burned area mapping. The Regional Burned Forest Mapping in Italy (ITALSCAR) project (Paganini et al. 2003), for example, produced burn scar maps for the period 1997–2000 using Landsat TM data. The Italian Ministry of the Environment used National Aeronautics and Space Administration (NASA) *Terra* Advanced Spaceborne Thermal Emission and Reflection Radiometer (ASTER) data and *SPOT 4–5* High-Resolution Visible Infrared (HRVIR) images to provide detailed information on burned area perimeters in the Italian national parks for the period 2001–05 (Brivio et al. 2009; Petrucci et al. 2010).

In Mediterranean environments such as those described above, regional fire monitoring can rely only on HR images (Koutsias et al. 1999). Global Monitoring for Environment and Security (GMES; available online at http://www.gmes.info) operational services, devoted to postfire estimates of damage and loss of natural resources, are specifically based on HR data (available online at http://www.riskeos.com).

Several methods have been developed for mapping fire-affected areas from multitemporal or single postfire satellite images: supervised classifications (i.e., maximum likelihood, decision tree, and neural network; Silva et al. 2005; Kontoes et al. 2009; Brivio et al. 2003), linear transformations (i.e., tasselled cap and principal component analysis; Patterson and Yool 1998; Hudak and Brockett 2004), spectral unmixing techniques (Román-Cuesta et al. 2005; Smith et al. 2007), and logistic regression models (Koutsias and Karteris 2000). Techniques based on thresholding the spectral indices (SIs) are widely applied, because they are computationally fast and efficient to detect fire-affected areas with both MR and HR data (Chongo et al. 2007; Smith et al. 2007). However, no agreement exists on which index performs best and in which conditions it has to be preferred (Lasaponara 2006). Moreover, threshold values are not constant and sometimes require to be tuned for the different environments or even adapted to local conditions or from scene to scene (Barbosa et al. 1999; Smith et al. 2007).

The objective of our research was to develop a new algorithm for mapping fire-affected areas in a Mediterranean environment from postfire HR satellite images. The algorithm integrates multiple SIs to exploit the complementary and/or the redundant information brought by each of them and to avoid the a priori selection of the most suitable one. Moreover, to overcome the need of tuning crisp thresholds locally or from scene to scene, each index is mapped into degrees of membership of burning by exploiting fuzzy sets theory (Zadeh 1965). The proposed algorithm has
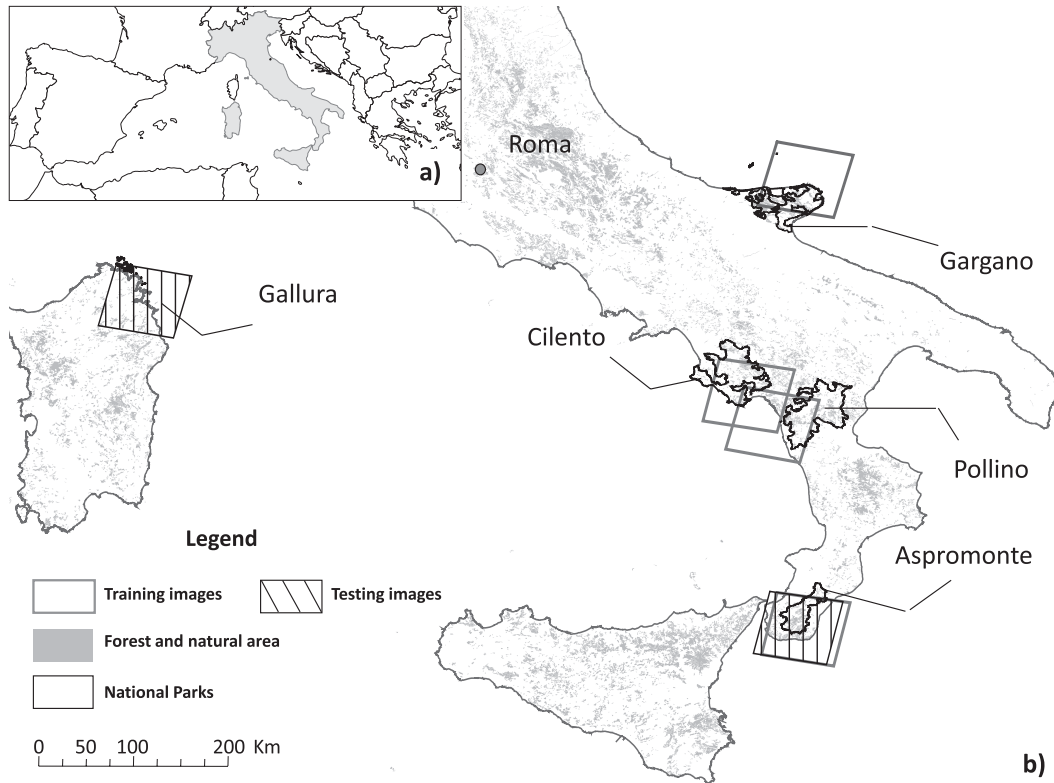
Figure 1. (a) Study area, Southern Italy and Sardinia in the Mediterranean basin, and (b) spatial distribution of ASTER images used as training and test dataset.

been calibrated with training data extracted from a set of ASTER images and automatically applied to other images of Southern Italy to assess its performance.

2. Study area and imagery dataset

The study area (Figure 1) covers Southern Italy, where the greatest damage caused by fires to natural ecosystems is within protected areas (Ministero dell'Ambiente 2008). For calibration and validation, ASTER images (AST07 product) were selected over the Italian national parks most affected by fire (Figure 1) to cover different Mediterranean natural environments (Brivio et al. 2009). One scene, selected over the Gallura (GAL) region (Sardinia), was added to assess the performance of the methodology in a different location dominated by the typical "macchia Mediterranea." All images were selected in late summer (July–September) to maximize the number of observed burned areas and to cover the entire fire season of different years. The choice of multiple scenes acquired over different sites and in different years makes both training the algorithm and validation of its performance robust with respect to application to other sites and/or periods. Table 1 gives the dominant land-cover classes where fires occurred for each site as derived from the Corine land-cover (CLC) map (available online at http://www.eea.europa.eu/publications/COR0-landcover).

Table 1. ASTER images used for training (15 874 pixels) and validation (120 950 pixels) and the dominant CLC classes where fires occurred. The classes of land cover for agriculture are arable land (CLC 2.1), permanent crops (olive trees; CLC 2.2), and heterogeneous agricultural areas (CLC 2.4). The classes of land cover for forest/other wooded are forest (CLC 3.1) and scrub and/or herbaceous vegetation associations (CLC 3.2).

	Image date	No. of polygons	No. of pixels	Avg area (ha)	Std dev (ha)	Min (ha)	Max (ha)	Land cover (%)
Training areas								
Aspromonte	8 Sep 2001	20	5408	13.4	21.0	1.3	96.5	Agriculture (72)
Gargano	20 Jul 2001	14	2333	10.0	20.2	1.4	79.0	Agriculture (81)
Pollino	14 Sep 2004	9	5987	7.1	4.5	1.8	14.8	Forest/other wooded (83)
Cilento	5 Sep 2003	14	2146	6.0	3.5	1.4	12.5	Forest/other wooded (44) Agriculture (32)
Test areas								
Aspromonte (ASP1)	12 Jul 2003	—	—	—	—	—	—	—
Aspromonte (ASP2)	28 Jul 2003	143	93870	14.7	48.0	1.0	547.2	Agriculture (51) Forest/other wooded (29)
Gallura	27 Jul 2005	31	25827	23.2	44.02	1.1	207.1	Forest/other wooded (47) Agriculture (46)

The AST07 product is composed of surface reflectance in the visible (VIS; green, band 1: 0.52–0.60 μm; red, band 2: 0.63–0.69 μm) and near-infrared (NIR) wavelengths (band 3: 0.78–0.86 μm) with a resolution of 15 m, and shortwave IR (SWIR) wavelengths (band 4: 1.6–1.7 μm; band 5: 2.14–2.18 μm; band 6: 2.18–2.22 μm; band 7: 2.23–2.28 μm; band 8: 2.29–2.36 μm; band 9: 2.36–2.43 μm) with a spatial resolution of 30 m. Each scene is 60 km wide across track. The ASTER instrument is on board the NASA *Terra* spacecraft (repeat cycle 16 days), and data acquisition is based upon requests (on demand). This is the major drawback of the instrument for operational applications (Yamaguchi et al. 2001).

Availability of red, NIR, and several SWIR bands allows us to calculate SI usually adopted for burned area mapping. The spatial resolutions of 15 m (VIS-NIR) and 30 m (SWIR) are suitable to detect burns of about few hectares typical of the Mediterranean regions (Kontoes et al. 2009).

ASTER data were preprocessed to register and resample SWIR bands to the higher spatial resolution of the VIS-NIR bands. Four images were used for training, and the remaining three were used to test the performance [Aspromonte (ASP) test area] and the generalizing capacity (Gallura test area) of the algorithm. The Aspromonte test dataset is constituted by two ASTER images acquired over the same area with a 16-day interval that allows the identification of fires occurred between the two acquisition dates. In this way, it was possible to test the method performance on recent (less than 30 days) fire-affected areas and to compare it to segmentation based on the SIs performed by tuning locally each index thresholds. For the Gallura image, field ancillary fire information (coordinates, date of fire

Table 2. Spectral indices adopted and references to recent applications for burned area mapping: $\alpha = 0.1$, $\beta = 0.6$, and $L = 0.5$.

	Spectral index	Equation	Reference
NIR	Near-infrared	ρ_{NIR}	Pereira 1999
CSI	Char soil index	ρ_{NIR}/ρ_{SWIR8}	Smith et al. 2005
NBR	Normalized burn ratio	$(\rho_{NIR} - \rho_{SWIR8})/(\rho_{NIR} + \rho_{SWIR8})$	Key and Benson 1999
BAI	Burn area index	$[(\alpha - \rho_{RED})^2 + (\beta - \rho_{NIR})^2]^{-1}$	Chuvieco et al. 2002
SAVI	Soil-adjusted vegetation index	$(\rho_{NIR} - \rho_{RED})(1 + L)/(\rho_{NIR} + \rho_{RED} + L)$	Chuvieco et al. 2002
MIRBI	Mid-infrared burn index	$10 \times \rho_{SWIR5} - 9.5 \times \rho_{SWIR4} + 2$	Trigg and Flasse 2001

events, and an approximate estimate of the burned area) were made available by the Corpo Forestale dello Stato (CFS).

3. Methods

3.1. Concept of the approach

The methodology proposed in this paper is based on a multicriteria approach able to integrate into a synthetic score the results obtained with several spectral indices. The basic and simple idea is the reinforcement of evidence: the more signs of burn (provided by the indices and interpreted with fuzzy membership functions) that are seen in the observed data, the higher the synthetic score of the burn class. The theoretical framework is fully described by Carrara et al. (Carrara et al. 2008) and Stroppiana et al. (Stroppiana et al. 2009a). The advantage offered by fuzzy sets is to convert spectral indices into a common domain [0, 1] through fuzzy membership function and to use soft rather than crisp constraints for the indices. The methodology proposed in this paper relies on previous experiments done on the same study area with ASTER data that showed the complementarities of different SI, and it constitutes a methodological development of these experiences (Zaffaroni et al. 2007; Brivio et al. 2009; Stroppiana et al. 2009b). We computed from the ASTER bands indices commonly used for burned area mapping in the Mediterranean environment and specifically tested for Southern Italy (Lasaponara 2006; Table 2).

In particular, Stroppiana et al. (Stroppiana et al. 2009b) showed that none of these indices [normalized burn ratio (NBR), burn area index (BAI), NIR, char soil index (CSI), soil-adjusted vegetation index (SAVI), and mid-infrared burn index (MIRBI)] can be considered the best choice for identifying burned surfaces without misclassification with other targets as shown by the results of a separability analysis for different SIs as reported in Stroppiana et al. (Stroppiana et al. 2009b; Table 3). A similar ranking of the indices derived from SPOT-VGT data was reported by Lasaponara (Lasaponara 2006).

Each index performs well in separating burns from one or at maximum two classes of unburned surfaces but at the same time leads to confusion with the others. This remark strengthens the idea of a multicriteria approach able to integrate the different and complementary information brought by the indices.

Figure 2 shows the flowchart of the methodology. Step 1 consists in the calculation of the SIs from the multispectral data. SIs are then converted into membership degrees (step 2) using fuzzy membership functions *f*, which are parameterized from the analysis of the training data with a partially data-driven approach (Robinson

Table 3. Measure of separability (*S*) between burned areas and the other surfaces for the different spectral indices. The numbers set in boldface refer to the highest separability for each surface.

	NBR	BAI	NIR	CSI	SAVI	MIRBI
Vegetation	**1.99**	1.63	1.55	1.74	1.87	1.38
Shadow	**1.74**	0.53	0.42	1.67	1.19	0.20
Soil	1.10	1.42	1.50	1.01	0.92	**1.54**
Unburned (average)	**1.61**	1.20	1.16	1.47	1.33	1.04
Unburned (Lasaponara 2006)	**1.34**	1.12	1.02	—	1.28	—

2003). Once the SIs are reduced to a common domain [0, 1], the membership degrees are combined into a synthetic score (step 3) by applying a weighted average (WA) operator. The WA map represents a synthetic continuous degree of likelihood of burn which is used to identify the clusters of core pixels (seeds) considered highly probable to be burned (WA score > 0.7; step 4). The final map, WA region growing (WA_RG; step 5), is obtained by applying a region-growing algorithm (IDL, ITT Visual Information Solutions) that identifies all pixels that are connected neighbors to the seed pixels and fall within a range of 3 times the standard deviation ($\pm 3\sigma$) of the seeds score values. A postclassification clumping filter, 3×3 pixels, has been applied to the classification map and results converted to vector format; finally, small area polygons (size < 1 ha) have been eliminated. In this flowchart, the membership functions *f*, defined from the training burned pixels, are assumed to be fixed, and all steps of the methodology can be automatically implemented to classify ASTER images with no further intervention or supervision.

The next subsections describe in detail the data handling conducted on the different stages of the methodology and for the validation exercise.

3.2. Fuzzy membership functions definition

The construction of the fuzzy membership functions of each index is based on a partially data-driven approach that uses statistical analysis of the training data and expert knowledge. Frequency distribution of each SI values of the training perimeters selected by photo interpretation (more than 15 000 pixels) were interpolated with a
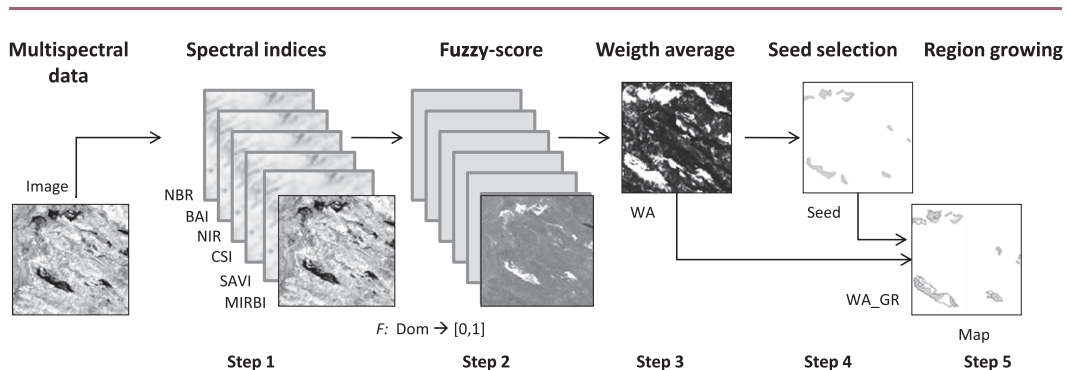
Figure 2. Steps of the proposed mapping procedure.

sigmoid curve, and least squares fitting provided the parameters μ and σ of the membership functions. Likelihood of burn is described by a decreasing curve for NBR, NIR, CSI, and SAVI [Equation (1a)] and by an increasing one for BAI and MIRBI [Equation (1b)]:

$$f = 1 + \exp\left[\left(\frac{\text{SI} - \mu}{\sigma}\right)\right]^{-1} \quad \text{and} \tag{1a}$$

$$f = 1 + \exp\left[-\left(\frac{\text{SI} - \mu}{\sigma}\right)\right]^{-1}. \tag{1b}$$

The functions map SI values into the [0, 1] range where the higher the likelihood of burn, the closer the score is to 1. The SI values belonging to the smoothed tails of the function cover the area where the commission errors are likely to occur (confusion with other surface targets). Expert knowledge has been used to set thresholds to the membership functions for SI values where burned area theoretically should tend and/or should not exist in the spectral domain. The threshold values for the different functions have been derived by Stroppiana et al. (Stroppiana et al. 2009b).

3.3. Fuzzy degree aggregation

The synthetic indicator is created by aggregation of the SI fuzzy membership degrees which, in this case, is done with a WA operator. Weights (relative importance of each index) have been set based on the average separability measures of Table 3. This study has improved the approach proposed by Stroppiana et al. (Stroppiana et al. 2009b); the SI burned membership functions have been derived by a partially data-driven approach thanks to the analysis of a more consistent training of spectral response of burn areas. Moreover, the mapping method here described adopts an automatic WA_RG procedure that starts from seed pixels selected on the base of the synthetic fuzzy indicator final score.

3.4. Validation

For validation we used an independent set of ASTER images (Aspromonte in 2003; Gallura in 2005). For the Aspromonte test area, the maps produced for the first (12 July 2003) and second (28 July 2003) date were subtracted to obtain the fire events that occurred only in the period between the two acquisitions. All the classification maps were compared with the polygons identified by photo interpretation to derive the error matrix and the accuracy measurements including overall accuracy (OA), kappa (K) statistics, and omission/commission errors (Congalton 1991).

The final maps were also compared to classifications obtained from single index thresholding with values adapted for each scene. Among the various techniques presented in the literature, we used a common approach based on thresholds of SI

values. Several authors (Smith et al. 2007; Barbosa et al. 1999) propose to define SI threshold values calculating mean μ and standard deviation σ of the index values from training data and to classify as burned each pixel of the image that falls in the range $\mu \pm 2\sigma$. In our case, statistics were extracted from a subsample of about 400 pixels, belonging to different photo-interpreted polygons of the Aspromonte 2003 and Gallura 2005 test images. BAI and MIRBI, following Smith et al. (Smith et al. 2007), used the thresholds previously derived by Stroppiana et al. (Stroppiana et al. 2009b) for ASTER adapting the values proposed by Chuvieco et al. (Chuvieco et al. 2002) and Trigg and Flasse (Trigg and Flasse 2001). All the maps were filtered with a 3 × 3 median filter, and only polygons greater than 1 ha were considered as fire-affected areas; finally, the Corine land-cover map was also used for masking out artificial surfaces (CLC 1), bare rocks (CLC 3.3.2), and coastal wetlands (CLC 4.2).

4. Results and discussion

4.1. Fuzzy functions

Figure 3 shows the normalized frequency histograms for each SI as extracted from the training dataset. The bottom row of the figure shows the histograms of all data pulled together and the sigmoid derived by interpolation that will define the index membership function. Values of the spectral indices covering different domains (*x* axis) are all mapped in the range [0, 1] on the *y* axis. Variability of vegetation characteristics, intensity and duration of the fires and the regrowth processes, which occur between the fire event and satellite acquisition, lead to different postfire spectral responses over the sites which are highlighted by the variability of the histograms.

Table 4 shows the parameters of the membership functions for each index. The fuzzy functions describe the degree of likelihood of burn by taking into account uncertainty with a smoothed curve in correspondence of the less frequent values where confusion with other surfaces is likely to occur. The functions have been constrained to $f = 0$ for SI values above or below the pixels that are not considered burned.

The contribution of each SI to the final score, quantified as the weight of the index in the computation of the synthetic indicator, was derived from their ability in separating burned areas from other surfaces (see Table 3). NBR is the most important index and contributes 21% of the final score, followed by CSI (19%) and SAVI (17%). The lowest weight was assigned to MIRBI (13%), and BAI and NIR complete the vector with an importance of about 15% each.

4.2. Maps of membership degrees and their integration

Figure 4 presents two examples of the fuzzy membership degree map for each index compared to the WA and WA_RG aggregated maps over the Aspromonte national park. The examples were chosen over areas where cloud shadows (Figure 4a) and bare soil (Figure 4b) might cause misclassification errors. In the figure, burned areas (white polygons in the RGB color composite) are identified by the
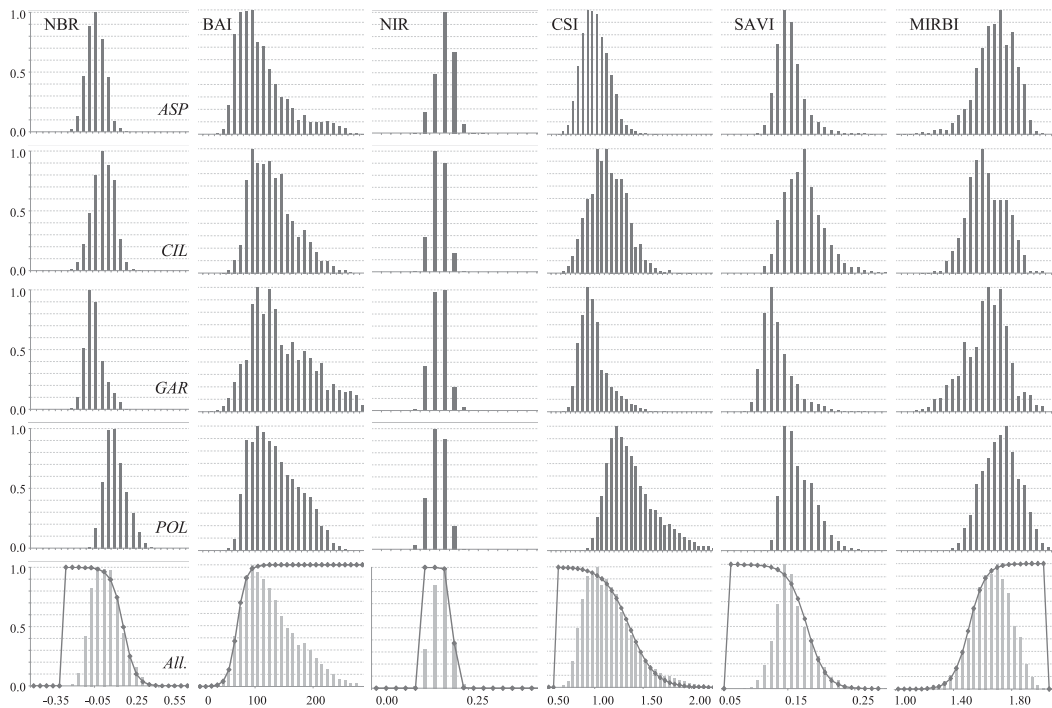
Figure 3. Frequency histograms of spectral indices values derived from the four training areas, Aspromonte (ASP), Cilento (CIL), Gargano (GAR), and Pollino (POL), and fuzzy memberships (continuous line) produced by interpolation of global histograms. The *y* axis shows normalized frequency distribution values (0–1), and the *x* axis illustrates the domain of the SIs considered.

highest membership degrees of all the indices (yellow to red colors) as a consequence of the definition of the fuzzy functions (see Figure 3); if a burned area has a consistently high degree for all indices, it will be assigned a high synthetic final score (convergence) and therefore it will be mapped as probably burned in the WA map. On the contrary, surfaces with high scores for only some of the indices, which is the case of unburned surfaces that are spectrally confused with burns, will have lower final scores and, for the compensation effect, will be likely classified as unburned in the final map. An example is given by the membership degree maps for the SAVI and MIRBI indices of Figure 4a: besides burned areas, high degrees are assigned also to clouds in the SAVI map and unburned vegetation and cloud

Table 4. Parameters of the fuzzy membership functions.

	NBR[a]	BAI[b]	NIR[a]	CSI[a]	SAVI[a]	MIRBI[b]
μ	0.20	63.90	0.20	1.34	0.17	1.49
σ	0.05	7.62	0.00	0.13	0.01	0.05
t[c]	≤ -0.3	—	≤ 0.1	≤ 0.55	≤ 0.05	≥ 2.0

[a] Decreasing sigmoid function.
[b] Increasing sigmoid function.
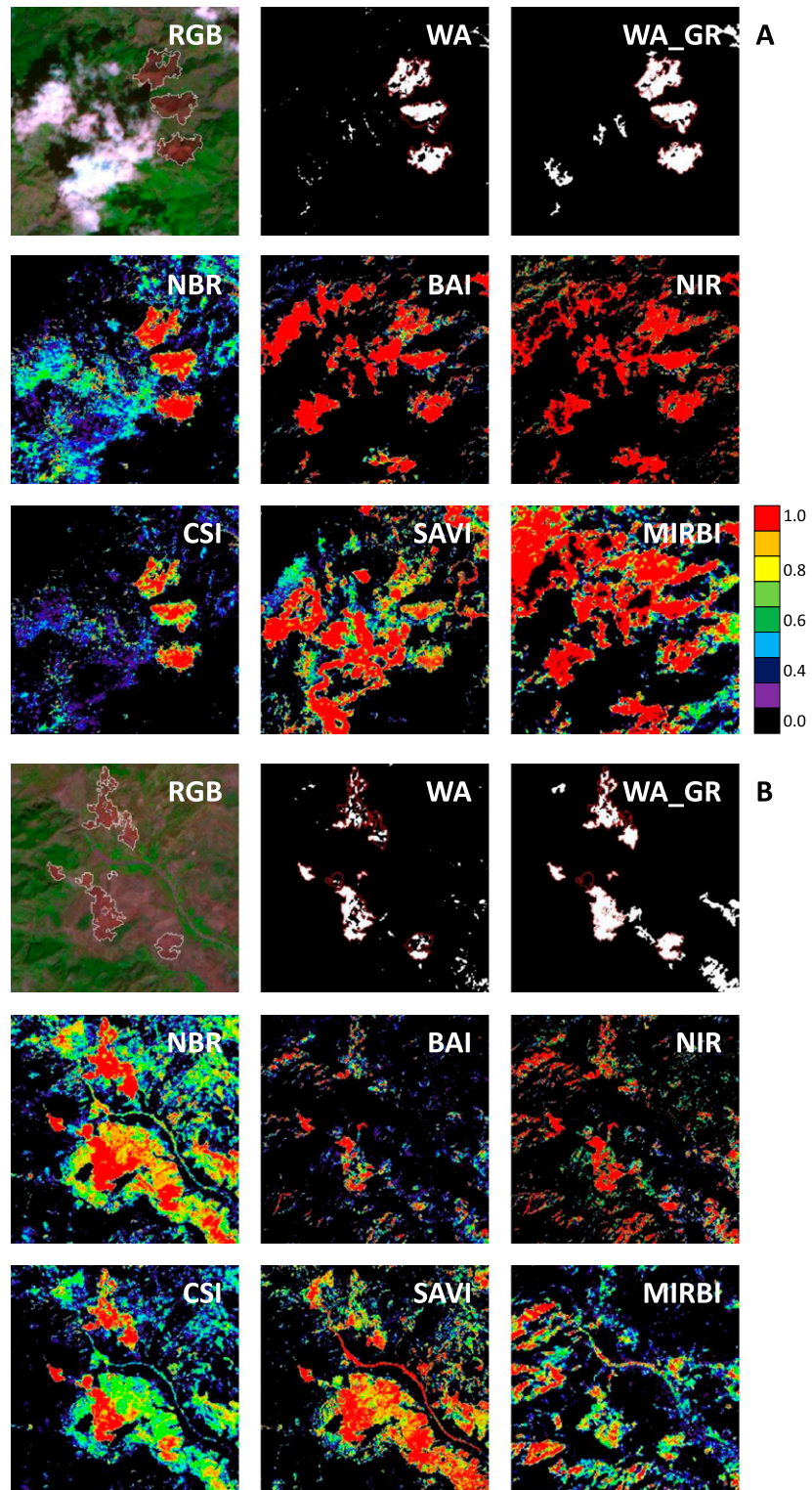[c] Threshold values (Stroppiana et al. 2009b) where function returns to zero score.

Figure 4. Example of SI membership degrees for two problematic areas, (a) cloudy and (b) sparsely vegetated, and burned area maps obtained by WA and WA_RG approaches. ASTER RGB: 832, where B8 = 2.336 μm, B3 = 0.8070 μm, and B2 = 0.6610 μm. Burn areas are marked by white polygons.

shadows in the MIRBI map. Because the same targets have low degrees in the other indices, the final aggregated map (WA) is free of these misclassification errors.

Similarly, NBR can discriminate cloud shadows from burns but produces errors over bare soil surfaces (membership degree > 0.7), as seen in Figure 4b. BAI behaves the opposite way by producing greater errors for cloud shadows (degree > 0.9) as seen in the top example area. CSI performs better in conditions of bare soil, where its degree is lower than NBR's. NIR produces intermediate results with some confusion with clouds (Figure 4a) and topographic shadows (Figure 4b). MIRBI and SAVI have also major problems for bare soil and water. In the synthetic indicator (WA), the higher scores (>0.7) are in correspondence of the photo-interpreted burned perimeters (red boundaries). In this way, the complementary behavior of the indices, such as in the case of NBR and BAI with respect to cloud shadows, allows the compensation of misclassification and the reduction of the global commission error. Finally, the region-growing algorithm (WA_RG) improves the results by exploiting local automatically adapted thresholds derived from burn seeds statistics. Although WA_RG can produce some artifacts, the main effect is to enhance areas in the image that are related to burned areas (Figure 4b).

4.3. Burned area maps and validation

Figure 5 shows the distribution of burned areas derived by photo interpretation (Figure 5a) and the results of the WA_RG classification (Figure 5b) for the test images of Aspromonte (top) and Gallura (bottom). In both cases, fire-affected areas (FAA) are mainly located near the coast, where human-induced fire risk is higher because of higher population density and easy accessibility.

No systematic error patterns are evident in the classification (i.e., fires are detected over the entire territory and across all land covers that are subject to burning), confirming that the method is robust; however, some underestimation is observed in the classified maps. The WA_RG method was able to identify, partially or totally, the majority of photo-interpreted polygons in both the test sites. In the Aspromonte image, 84 polygons out of the 143 events were identified: these polygons cover about 92% of the total area burned (2098 ha). The undetected polygons are characterized by an average size of 2.7 ha (median 2.0 ha), which is smaller compared to the detected ones (average 23.1 ha, median 7.74 ha). The size of the burned areas is one of the factors that can influence the underestimation error (i.e., omission); among all, the geometric characteristics of the satellite sensor (i.e., spatial resolution) limit the minimum size of fire events that can be detected and therefore the rate of omission errors. Similarly, in the Gallura test image, the algorithm was able to detect 26 polygons (average 22.0 ha, median 4.66 ha), corresponding to 96% of the total area burned. Also in this case, the undetected fire events are small (average 4.0 ha, median 2.86 ha) compared to the image spatial resolution.

The results of the validation of the WA_RG maps are summarized in Table 5, where the performance of the automated algorithm is also compared to classifications obtained by thresholding the SIs; almost all of the classifications have an OA $> 99\%$ (data not shown). Results are ranked based on the K statistic of the confusion matrix. The WA_RG classifications for both validation sites performs
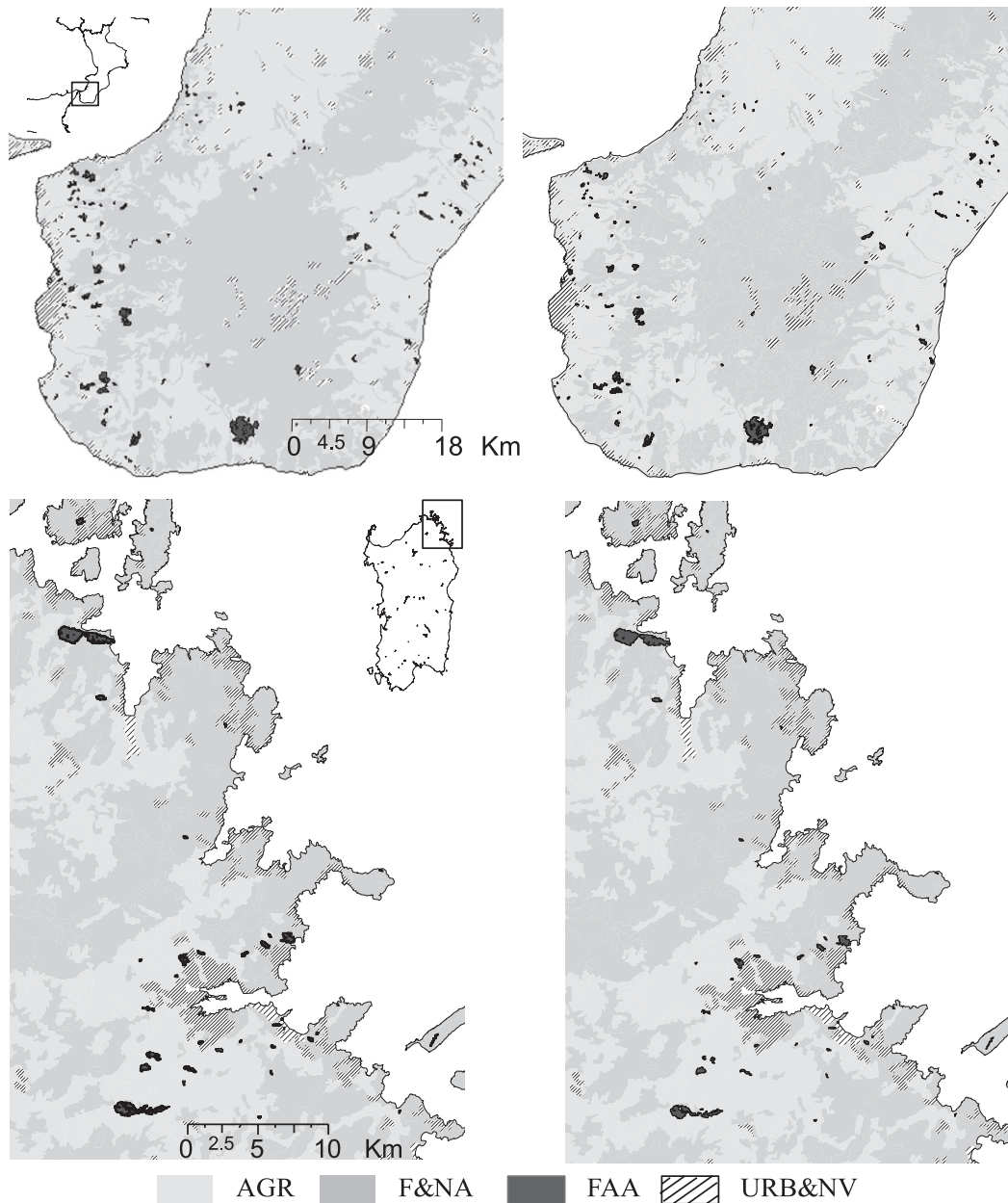
Figure 5. Reference map from (left) photo-interpretation and (right) classification results for the two test images: (top) ASP and (bottom) GAL. Burn polygons are superimposed to the CLC classes grouped in broad categories: AGR, forest and natural area (F&NA), fire affected area (FAA), and urban and not vegetated (URB&NV).

well with $K > 75\%$ and as high as 87% in the case of the Gallura validation site. The method shows to be conservative (i.e., low rate of false alarms) with commission errors of 3.56% and 9.36%, respectively, for Aspromonte and Gallura. Omission errors (37.29% in Aspromonte and 16.57% in Gallura) are comparable or

Table 5. Accuracy measures derived from the error matrix for the two test images for the different methods. The asterisk refers to the use of fixed thresholds.

Location	Method	K	Commission (%)	Omission (%)
Aspromonte	WA_RG	0.76	3.56	37.29
	NBR	0.75	10.81	35.39
	CSI	0.74	8.49	36.86
	NIR	0.71	18.88	36.84
	MIRBI*	0.59	32.80	45.07
	SAVI	0.28	79.02	51.72
	BAI*	0.08	65.14	95.43
Gallura	WA_RG	0.87	9.36	16.57
	NBR	0.84	1.15	27.13
	CSI	0.83	0.87	27.99
	BAI*	0.52	22.91	60.06
	MIRBI*	0.2	87.67	26.61
	SAVI	0.07	95.59	29.52
	NIR	0.02	97.91	20.87

even lower than values obtained from the classification derived by image thresholding of the SIs with scene-adapted thresholds.

The rate of omission over the Aspromonte site is higher but comparable to omissions of the NBR, NIR, and CSI indices, thus suggesting that spectral separability of the image targets is intrinsically difficult to be achieved. In fact, the numerous burned polygons (143) extracted from the photo interpretation cover a wide range of spectral characteristics, and the indices perform in a very different way with lower accuracy. However, the aggregation of the single index membership degrees coupled with a region-growing algorithm (WA_RG) does improve the classifications obtained by thresholding the single SI images especially if we keep in mind that WA_RG has been applied automatically to the validation images, and it did not require the time-consuming effort of tuning thresholds scene by scene. In the Gallura site, the WA_RG is better than any other classification.

The order with which the classifications appear in Table 5 confirms that the performance of the SIs strongly depend on the scene characteristics. As previously discussed, the Gallura image is characterized by a high spectral separability between burned and unburned surfaces, and therefore classification accuracy is higher (NBR: OA > 99%, $K = 0.84$), with an almost negligible commission error (about 1%). The minimum commission error in the Aspromonte site is obtained by the WA_RG algorithm followed by the CSI index. Among the indices, NBR and CSI provide good and consistent results in the two test sites (OA > 99%; $K > 0.74$) being at the top of the ranking list. On the contrary, NIR is one of the best choices for Aspromonte (OA > 99%, $K = 0.71$) but performs badly over Gallura (OA = 68.72%, $K = 0.02$). BAI and MIRBI show inconsistent performance: BAI presents the worst accuracy measures for Aspromonte and MIRBI presents one of the worst for Gallura. Note that, for BAI and MIRBI, we have used fixed thresholds, available in literature, whereas the maps produced from the other indices were derived by tuning the threshold on 400 pixels extracted from each test image.

Table 6 shows SI statistics computed over the burned sampled pixels and the thresholds used for classification of each test image. The greatest variability of the SI values is observed from one site to another but also from scene to scene over

Table 6. Statistics extracted for each index from the test images: ASP1 (12 Jul 2003), ASP2 (28 Jul 2003), and GAL (27 Jul 2005). Values of thresholds (T_{min} and T_{max}) used for mapping burned areas with the single index approach.

|			NBR	BAI*	NIR	CSI	SAVI	MIRBI**
Statistics	Min/max	ASP1	−0.18/0.31	27.57/240.38	0.12/0.24	0.70/1.90	0.10/0.24	1.49/1.99
		ASP2	−0.16/0.17	38.38/234.03	0.12/0.22	0.72/1.41	0.09/0.20	1.50/1.95
		GAL	−0.21/0.08	20.76/240.56	0.12/0.27	0.66/1.17	0.10/0.23	1.38/1.89
	Mean/std	ASP1	0.05/0.06	111.28/39.45	0.16/0.02	1.11/0.13	0.13/0.02	1.79/0.09
	dev	ASP2	−0.01/0.06	107.09/39.86	0.16/0.02	0.98/0.12	0.12 /0.01	1.77/0.10
		GAL	−0.09/0.05	90.32/52.68	0.17/0.03	0.84/0.08	0.14/0.02	1.60/0.11
Thresholds	T_{min}/T_{max}	ASP1	−0.07/0.17	32.38/190.17	0.12/0.20	0.85/1.38	0.10/0.16	1.62/1.97
		ASP2	−0.13/0.11	27.37/186.80	0.12/0.20	0.75/1.22	0.09/0.14	1.57/1.97
		GAL	−0.18/0.01	−15.03/195.67	0.12/0.23	0.68/1.00	0.10/0.19	1.38/1.82

* Fixed value is 150.
** Fixed value is 1.5.

the same site; SI values change because they are observed on different dates such as in the case of Aspromonte. Because in this last case the geographical context involved is the same, the difference observed, for example, in the NBR values is mainly a consequence of the change in time of the postfire spectral signal; in fact, the second image is acquired 16 days after the first one. The high variability of the burned signal reduces the exportability of crisp thresholds for an automated application to different images (i.e., thresholds need always some adjustment that in the algorithm proposed here is performed by the use of fuzzy membership). In particular, the SI statistics suggest that the fixed literature values proposed for BAI (>150) and MIRBI (>1.5) may be not suitable for mapping burns in our geographical area. These figures confirm the site variability that clearly appears from the histograms of Figure 3.

Figure 6 shows the scatterplots of the classified WA_RG and reference photointerpreted polygons for Aspromonte (left) and Gallura (right). The WA_RG algorithm is able to accurately identify fire polygons ($r^2 > 0.98$) in both test images, although some underestimation occurs (regression line slope < 1). Because correlation between estimated and reference fire areas can be influenced by few large fires, we focused on burns with an area smaller than 50 ha (scatters on the inside box). Also, in this case, the comparison provides very good results and the regressions still have a high coefficient of determination ($r^2 = 0.8$); the Aspromonte case study shows an underestimation higher ($n = 84$, slope = 0.60) compared to Gallura ($n = 25$, slope = 0.7), where points are better aligned along the 1:1 line.

In this environment, larger burned areas are generally due to more intense fire events and are characterized by a more persistent spectral signal. Spectral separability of the burned areas is influenced by surface conditions, which are the result of the complex interactions between fire dynamics, prefire vegetation characteristics and conditions, vegetation regrowth after the fire, and the time between fire and image acquisition. Field information available for Gallura showed that a greater underestimation occurs for events further in time from image acquisition, although no statistically significant correlation resulted between the omission error and the time lag between fire and acquisition date (data not shown).

An example is given in Figure 7 that shows the classification of two largest (>100 ha) burned areas visible in the Gallura image. The more recent event
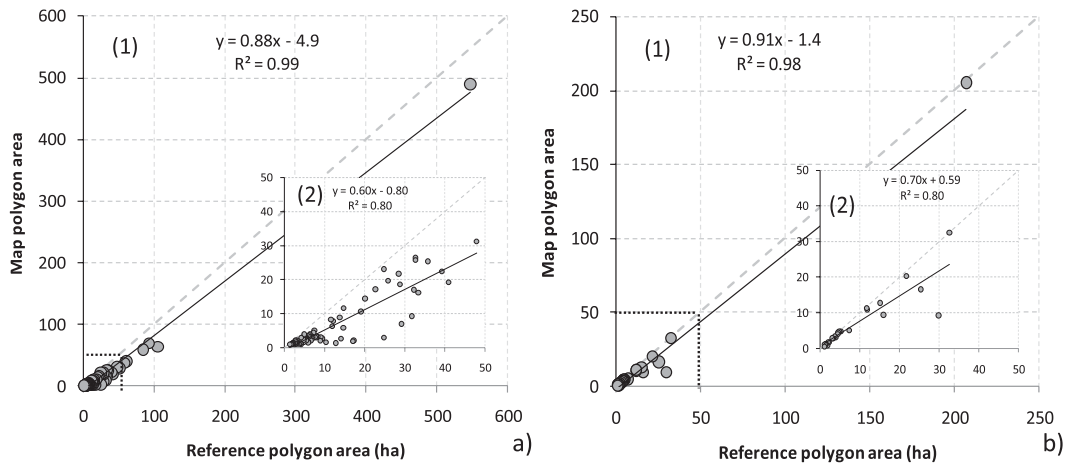
Figure 6. Reference burn polygons from the photo-interpretation and estimated burn area for the (a) ASP and (b) GAL test images. Shown for (a),(b) are 1) the entire dataset and 2) a zoom on smaller burned surfaces (<50 ha).

(Figure 7a), which occurred 4 days before image acquisition, shows a clear burned spectral signal in dense natural vegetation (CLC 3.2.3: sclerophyllous vegetation) where the fuzzy algorithm identified well unburned patches inside the burned perimeter. The second event (Figure 7b) is only partially detected, probably because after 20 days the burned signal is confused with the signal from sparse vegetation and bare soils [CLC 2.4.3: land principally occupied by agriculture (AGR) with significant areas of natural vegetation].

The analysis of the distribution of the fire events across the CLC classes highlighted that, in both regions, fires affected agricultural (51% Aspromonte and 46% Gallura) and forested/natural areas (46.2% Aspromonte and 52.5% Gallura) in similar proportions. In particular, the classes most affected by fires are heterogeneous agricultural areas (CLC 2.4; 28.2% Aspromonte and 26.7% Gallura) and scrub and/ or herbaceous vegetation (CLC 3.2; 34.5% Aspromonte and 50.9% Gallura). This regime is challenging for burned area mapping because of the characteristics of these two classes, which typically have low canopy coverage, where the burned signature is not persistent in time.

5. Conclusions

This work presents a novel approach for mapping burned areas with HR data in a Mediterranean environment of Southern Italy. The novelty is the integration into a synthetic indicator of spectral indices, which are converted to a common domain [0, 1] through fuzzy membership function. The indicator provides soft information on the likelihood of burn, where high scores are retrieved in condition of SIs convergence (reinforcement of evidence) and fuzzy degrees are used in combination with a region-growing algorithm (WA_RG). The advantages of integrating fuzzy degrees are (i) to reduce the effort involved in adapting thresholds from scene to scene, (ii) to exploit the complementary information brought by each index over
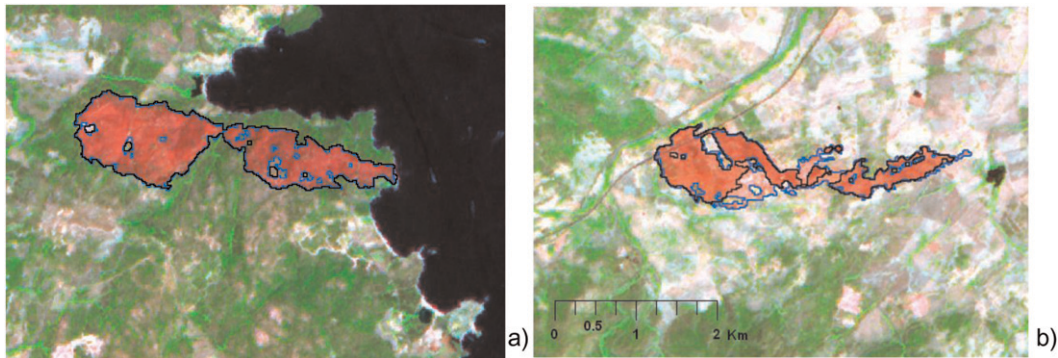
Figure 7. Classifications examples of two events in the GAL test image. Classification polygons (black line) and photo-interpreted area (blue line) are superimposed to ASTER RGB (832) images. Shown are (a) a situation with a predominant natural vegetation cover (CLC 3.2.3: sclerophyllous vegetation) and (b) a more heterogeneous agricultural situation (CLC 2.4.3: land principally occupied by AGR, with significant areas of natural vegetation).

targets of likely spectral confusion, and (iii) to improve reliability when applied to different geographical areas. The burned area maps obtained with the WA_RG algorithm over test sites are very accurate ($K = 0.75$ and $K = 0.87$), with a very low rate of false alarms (commission errors <10%). Omission errors are mainly due to undetected small areas; patches smaller than 3 ha are often missed, although these events account for a small proportion of the total burned area and do not influence the global accuracy. Even when tested in heterogeneous landscapes, where the pixel burned signal is contaminated by unburned vegetation and becomes weaker with time since fire, performance is as accurate as locally adapted SI threshold-based techniques. Compared to these techniques, the method is much faster, because it does not require tuning of the thresholds to the characteristics of the satellite scene and can be a candidate approach to the operational update of the geodatabase of fire-affected areas. However, the proposed approach to some extent depends on the parameterization of the fuzzy membership functions, which in this case is done with a partially data-driven approach to cover the wide range of spectral properties of burned areas in the Mediterranean environment of Southern Italy. Clearly, it can be applied automatically where these conditions are met, and further tests should be carried out if the algorithm has to be applied to different biomes. Indeed, this will be topic for future research as well as testing the performance with different high-resolution optical sensors (e.g., TM, SPOT) and on evaluating the exportability to the sensor of the new European Space Agency (ESA) Sentinel 2 mission, which is also devoted in the future for burned area mapping operational application (Drusch et al. 2010).

dello Stato (CFS) for providing field data and discussing the results. ASTER images were acquired thanks to the collaboration with the Department of Geography, University of Maryland. A particular thank you to Patricia Oliva (University of Alcalà de Henares, Spain) for the photo interpretation of the Aspromonte test images.

References

Arino, O., and J. M. Rosaz, 1999: 1997 and 1998 world ATSR fire atlas using ERS-2 ATSR-2 data. *Proc. Joint Fire Science Conf. and Workshop,* Boise, Idaho, University of Idaho and International Association of Wildland Fire, 177–182.

Barbosa, P. M., J. M. C. Pereira, and J. M. Grégoire, 1998: Compositing criteria for burned area assessment using multitemporal low resolution satellite data. *Remote Sens. Environ.,* **65,** 38–49.

——, J. M. Grégoire, and J. M. C. Pereira, 1999: An algorithm for extracting burned areas from time series of AVHRR GAC data applied at a continental scale. *Remote Sens. Environ.,* **69,** 253–263.

Brivio, P. A., M. Maggi, E. Binaghi, and I. Gallo, 2003: Mapping burned surfaces in Sub-Saharan Africa based on multi-temporal neural classification. *Int. J. Remote Sens.,* **24,** 4003–4018.

——, B. Petrucci, M. Boschetti, P. Carrara, M. Pepe, A. Rampini, D. Stroppiana, and P. Zaffaroni, 2009: A multi-year geographic database of fire affected areas derived from satellite images in the national parks of Italy. *Ital. J. Remote Sens.,* **41,** 65–78.

Camia, A., and Coauthors, 2009: Forest fires in Europe 2008. Joint Research Centre Scientific and Research Rep. 9, 88 pp.

Carrara, P., G. Bordogna, M. Boschetti, P. A. Brivio, A. Nelson, and D. Stroppiana, 2008: A flexible multi-source spatial-data fusion system for environmental status assessment at continental scale. *Int. J. Geogr. Inf. Sci.,* **22,** 781–799.

Catry, F. X., F. C. Rego, J. S. Silva, F. Moreira, A. Camia, C. Ricotta, and M. Conedera, 2010: Fire starts and human activities. Towards integrated fire management—Outcomes of the European project Fire Paradox, J. S. Silva et al. Eds., European Forest Institute Research Rep. 23, 9–21.

Chongo, D., R. Nagasawa, A. O. C. Ahmed, and F. Perveen, 2007: Fire monitoring in savanna ecosystems using MODIS data: A case study of Kruger National Park, South Africa. *Landscape Ecol. Eng.,* **3,** 79–88.

Chuvieco, E., M. P. Martìn, and A. Palacios, 2002: Assessment of different spectral indices in the red–near-infrared spectral domain for burned land discrimination. *Int. J. Remote Sens.,* **23,** 5103–5110.

Congalton, R. G., 1991: A review of assessing the accuracy of classifications of remotely sensed data. *Remote Sens. Environ.,* **37,** 35–46.

Drusch, M., F. Gascon, and M. Berger, 2010: GMES Sentinel 2 mission requirements document. European Space Agency Document, 42 pp. [Available online at http://esamultimedia.esa.int/docs/GMES/Sentinel-2_MRD.pdf.]

Dwyer, D., J. M. Gregorire, and J. P. Malingreau, 1998: A global analysis of vegetation fires using satellite images: Spatial and temporal dynamics. *Ambio,* **27,** 175–181.

French, N. H. F., E. S. Kasischke, and D. G. Williams, 2003: Variability in the emissions of carbon-based trace gases from wildfire in the Alaskan boreal forest. *J. Geophys. Res.,* **107,** 8151, doi:10.1029/2001JD000480.

Giglio, L., J. Descloitres, C. O. Justice, and Y. Kaufman, 2003: An enhanced contextual fire detection algorithm for MODIS. *Remote Sens. Environ.,* **87,** 273–282.

Hudak, A. T., and B. H. Brockett, 2004: Mapping fire scars in a southern African savannah using Landsat imagery. *Int. J. Remote Sens.,* **25,** 3231–3243.

Key, C. H., and N. C. Benson, 1999: Measuring and remote sensing of burn severity. *Proc. Joint Fire Science Conf. and Workshop,* Boise, Idaho, University of Idaho and International Association of Wildland Fire, Vol. 2, 284.

Kontoes, C. C., H. Poilvé, G. Florsch, I. Keramitsoglou, and S. Paralikidis, 2009: A comparative analysis of a fixed thresholding vs. a classification tree approach for operational burn scar detection and mapping. *Int. J. Appl. Earth Obs. Geoinformation,* **11,** 299–316.

Koutsias, N., and M. Karteris, 2000: Burned area mapping using logistic regression modeling of a single post-fire Landsat-5 Thematic Mapper image. *Int. J. Remote Sens.,* **21,** 673–687.

——, ——, A. Fernández, C. Navarro, J. Jurado, R. Navarro, and A. Lobo, 1999: Burnt land mapping at local scale. *Remote Sensing of Large Wildfires in the European Mediterranean Basin,* E. Chuvieco, Ed., Springer-Verlag, 123–138.

Lasaponara, R., 2006: Estimating spectral separability of satellite derived parameters for burned areas mapping in the Calabria region by using SPOT-Vegetation data. *Ecol. Modell.,* **196,** 265–270.

Ministero dell'Ambiente, 2008: Incendi boschivi nei parchi nazionali: Un decennio (1997-2006) di dati ''storici'' per meglio comprendere la situazione. L'anno 2007 per riflettere. 9 pp. [Available online at http://www.minambiente.it/opencms/export/sites/default/archivio/allegati/vari/incendi_boschivi_decennio.pdf.]

Mitri, G., and J. Gitas, 2006: Fire type mapping using object-based classification of Ikonos imagery. *Int. J. Wildland Fire,* **15,** 457–462.

Paganini, M., O. Arino, M. Benvenuti, M. Cristaldi, M. Bordin, C. Coretti, and A. Musone, 2003: ITALSCAR, a regional burned forest mapping demonstration project in Italy. *Proc. Int. Geoscience and Remote Sensing Symp. (IGARSS '03),* IEEE, Vol. 2, 1290–1292.

Patterson, M. W., and S. R. Yool, 1998: Mapping fire-induced vegetation mortality using Landsat Thematic Mapper data: A comparison of linear transformation techniques. *Remote Sens. Environ.,* **65,** 132–142.

Pereira, J. M. C., 1999: A comparative evaluation of NOAA/AVHRR vegetation indexes for burned surface detection and mapping. *IEEE Trans. Geosci. Remote Sens.,* **37,** 217–226.

Petrucci, B., B. Capitoni, R. Borelli, and F. Popolizio, 2010: ''Progetto Incendi'', portale cartografico nazionale del Ministero dell'Ambiente: Un esempio di gestione di dati cartografici a supporto dei piani antincendio boschivi nei parchi nazionali. *Foresta,* **7,** 13–21.

Pu, R., Z. Li, P. Gong, I. Csiszar, R. Fraser, W. M. Hao, S. Kondragunta, and F. Weng, 2007: Development and analysis of a 12-year daily 1-km forest fire dataset across North America from NOAA/AVHRR data. *Remote Sens. Environ.,* **108,** 198–208.

Robinson, V. B., 2003: A perspective on the fundamentals of fuzzy sets and their use in geographic information systems. *Trans. GIS,* **7,** 3–30.

Román-Cuesta, R. M., J. Retana, M. Gracia, and R. Rodríguez, 2005: A quantitative comparison of methods for classifying burned areas with LISS-III imagery. *Int. J. Remote Sens.,* **26,** 1979–2003.

Roy, D. P., Y. Jin, P. E. Lewis, and C. O. Justice, 2005: Prototyping a global algorithm for systematic fire affected area mapping using MODIS time series data. *Remote Sens. Environ.,* **97,** 137–162.

Silva, J. M. N., A. C. L. Sà, and J. M. C. Pereira, 2005: Comparison of burned area estimates derived from SPOT-VEGETATION and Landsat ETM+ data in Africa: Influence of spatial pattern and vegetation type. *Remote Sens. Environ.,* **96,** 188–201.

Simon, M., S. Plummer, F. Fierens, J. J. Hoelzemann, and O. Arino, 2004: Burnt area detection at global scale using ATSR-2: The GLOBSCAR products and their qualification. *J. Geophys. Res.,* **109,** D14S02, doi:10.1029/2003JD003622.

Smith, A. M. S., M. J. Wooster, N. A. Drake, F. M. Dipotso, M. J. Falkowski, and A. T. Hudak, 2005: Testing the potential of multi-spectral remote sensing for retrospectively estimating fire severity in African savanna environments. *Remote Sens. Environ.,* **97,** 92–115.

——, N. A. Drake, M. J. Wooster, A. T. Hudak, Z. A. Holden, and C. J. Gibbons, 2007: Production of Landsat ETM+ reference imagery of burned areas within southern African savannahs: Comparison of methods and application to MODIS. *Int. J. Remote Sens.,* **28,** 2753–2775.

Stroppiana, D., K. Tansey, J. M. Grégoire, and J. M. C. Pereira, 2003: An algorithm for mapping burnt areas in Australia using SPOT-VEGETATION data. *IEEE Trans. Geosci. Remote Sens.,* **41,** 907–909.

——, M. Boschetti, P. A. Brivio, P. Carrara, and G. Bordogna, 2009a: A fuzzy anomaly indicator for environmental monitoring at continental scale. *Ecol. Indic.,* **9,** 92–106.

——, ——, P. Zaffaroni, and P. A. Brivio, 2009b: Analysis and interpretation of spectral indices for soft multi-criteria burned area mapping in Mediterranean regions. *IEEE Geosci. Remote Sens. Lett.,* **6,** 499–503.

Tansey, K., and Coauthors, 2004: A global inventory of burned areas at 1 km resolution for the year 2000 derived from SPOT Vegetation data. *Climatic Change,* **67,** 345–377.

Thonicke, K., S. Venevsky, S. Sitch, and W. Cramer, 2001: The role of fire disturbance for global vegetation dynamics: Coupling fire into a Dynamic Global Vegetation Model. *Global Ecol. Biogeography,* **10,** 661–677.

Trigg, S., and S. Flasse, 2001: An evaluation of different bi-spectral spaces for discriminating burned shrub savanna. *Int. J. Remote Sens.,* **22,** 2641–2647.

Van der Werf, G. R., J. T. Randerson, L. Giglio, G. J. Collatz, and P. S. Kasibhatla, 2006: Inter-annual variability in global biomass burning emission from 1997 to 2004. *Atmos. Chem. Phys.,* **6,** 3423–3441.

Wooster, M. J., B. Zhukov, and D. Oertel, 2003: Fire radiative energy for quantitative study of biomass burning: Derivation from the BIRD experimental satellite and comparison to MODIS fire products. *Remote Sens. Environ.,* **86,** 83–107.

Yamaguchi, Y., H. Fujisada, A. B. Kahle, H. Tsu, M. Kato, H. Watanabe, I. Sato, and M. Kudoh, 2001: ASTER instrument performance, operation status, and application to Earth sciences. *Proc. Int. Geoscience and Remote Sensing Symp. (IGARSS '01),* IEEE, Vol. 3, 1215–1216.

Zadeh, L. A., 1965: Fuzzy sets. *Inf. Control,* **8,** 338–353.

Zaffaroni, P., D. Stroppiana, P. A. Brivio, and M. Boschetti, 2007: Utilizzo di immagini ASTER per la delimitazione di aree percorse da incendio. *Ital. J. Remote Sens.,* **39,** 93–101.